Variations in the ensemble of potassium currents underlying resonance in turtle hair cells

M. B. Goodman* and J. J. Art †‡

*Committee on Neurobiology, The University of Chicago, Chicago, IL 60637 and †Department of Anatomy and Cell Biology, University of Illinois College of Medicine, 808 South Wood Street, Chicago, IL 60612, USA

1. Potassium currents were characterized in turtle cochlear hair cells by whole-cell voltage clamp during superfusion with the potassium channel antagonists, tetraethylammonium (TEA) and 4-aminopyridine (4-AP). The estimated resonant frequency, f_0, was inferred from τ, the time constant of deactivation of outward current upon repolarization to −50 mV, according to the empirical relation, $f_0 = k_1\tau^{-1/2} + k_2$.

2. Dose–response relations for TEA and 4-AP were obtained by exposing single cells to ten concentrations exponentially distributed over four orders of magnitude. Potassium current in cells tuned to low frequencies was carried by a single class of channels with an apparent affinity constant, K_i, for TEA of 35·9 mM. Half-blocking concentrations of 4-AP were correlated with the time constant of deactivation and varied between 26·2 and 102 μM. In cells tuned to higher frequencies, K^+ current was carried by a single class of channels with high affinity for TEA ($K_i = 0{\cdot}215$ mM) and low affinity for 4-AP ($K_i = 12{\cdot}3$ mM). This pharmacological profile suggests that K^+ current in low frequency cells is purely voltage gated and in high frequency cells, it is gated by both Ca^{2+} and voltage.

3. For each current type, the voltage dependence of activation was determined from tail current amplitude at −50 mV. The purely voltage-gated current, $I_{K(V)}$, was found to increase e-fold in 4·0 ± 0·3 mV ($n = 3$) in low frequency cells exposed to TEA (25 mM). The Ca^{2+}- and voltage-gated current, $I_{K(Ca)}$, was more steeply voltage dependent, increasing e-fold in 1·9 mV ($n = 2$) in high frequency cells exposed to 4-AP (0·8 mM).

4. $I_{K(V)}$ was found to inactivate slowly during prolonged voltage steps (~10 s). Steady-state inactivation increased with depolarization from −70 mV and was incomplete such that on average $I_{K(V)}$ did not fall below ~0·39 of its maximum value.

5. Superfusion of 4-AP (0·8 mM) reversibly depolarized a low frequency cell and eliminated steady voltage oscillations, while TEA (6 mM) had no effect. In a high frequency cell, voltage oscillations were abolished by TEA, but not by 4-AP.

6. The differential pharmacology of $I_{K(V)}$ and $I_{K(Ca)}$ was used to measure their contribution to K^+ current in cells tuned to different frequencies. Both currents exhibited a frequency-dependent increase in maximum conductance. $I_{K(V)}$ accounted for nearly all K^+ current in cells tuned to less than 60 Hz, while $I_{K(Ca)}$ was the dominant current in higher frequency cells.

7. Mapping resonant frequency onto epithelial position suggests an exponential relation between K^+ current size and position. $I_{K(V)}$ appeared to be limited to the apical or low frequency portion of the basilar papilla and coincided with maximal expression of a K^+-selective inward rectifier, $I_{K(IR)}$. This finding is consistent with the notion that low frequency resonance is produced by interaction of $I_{K(V)}$ and $I_{K(IR)}$ with the voltage-gated Ca^{2+} current, I_{Ca}, and the cell's capacitance. The ionic events underlying higher frequency resonance are dominated by the action of $I_{K(Ca)}$ and I_{Ca} and include a contribution from $I_{K(IR)}$.

‡ To whom correspondence should be addressed.

A unifying feature of the elongated auditory epithelium is its tonotopic organization. In principle, tonotopy could reflect the spatial arrangement of tuned hair cells, mechanical tuning of the underlying basilar membrane, or both. In turtle, the distribution of electrically tuned hair cells is paramount since sound evokes a relatively uniform, frequency-independent displacement of the basilar membrane (O'Neill & Bearden, 1995). Resonant frequencies increase along the length of the sensory epithelium, varying from about 40 Hz at the apex to about 500 Hz in the intact cochlea (Crawford & Fettiplace, 1980). Variations in resonant frequency can be explained by changes in the amount and kinetics of the K^+ current (Art & Fettiplace, 1987; Wu, Art, Goodman & Fettiplace, 1995). A fundamental question concerns to what extent this variation is explained by a single class of K^+ channels. The contribution of large Ca^{2+}-activated K^+ channels (BK channels) to resonance is well-established (Lewis & Hudspeth, 1983; Art & Fettiplace, 1987) and similar channels are found in most hair cells. Additional K^+ currents, akin to delayed rectifiers and inactivating, 'A'-type currents, have been reported in a variety of cochlear and vestibular hair cells (Lewis & Hudspeth, 1983; Lang & Correia, 1989; Housley, Norris & Guth, 1989; Sugihara & Furukawa, 1989; Fuchs & Evans, 1990; Kros & Crawford, 1990; Murrow, 1994), but their functional role is unclear. One possibility is that low frequency resonance employs purely voltage-gated K^+ channels (K_V channels), a notion supported by the observation that outward current persists in low frequency hair cells when exposed to a saline containing only 1 μM Ca^{2+} (Art, Fettiplace & Wu, 1993).

The primary goal of the present work was to determine the ensemble of K^+ current types underlying resonance at different frequencies. We used wide-spectrum K^+ channel antagonists, tetraethylammonium (TEA) and 4-aminopyridine (4-AP), to determine if hair cells tuned to different frequencies expressed one or more K^+ channel types. The experimental design relied on the fact that most, if not all, K^+ channels are sensitive to these agents, and the notion that the existence of multiple K^+ channel types would result in single-cell dose–response relations different from those expected for a single class of binding sites. Our results show that the size and type of K^+ currents expressed in hair cells varies systematically with resonant frequency and, hence, position in the cochlea. In addition, we provide evidence that low frequency resonance is achieved by a distinct mechanism involving the interaction of a voltage-gated calcium current, a K^+-selective inward rectifier and a purely voltage-gated K^+ current. Preliminary accounts of some of the results have appeared (Goodman & Art, 1994; Goodman, 1995; Wu *et al.* 1995).

METHODS

Preparation and recording methods

Methods for isolating hair cells were similar to those described previously (Art & Fettiplace, 1987). Turtles (*Trachemys scripta elegans*; carapace length, 9–12 cm) were decapitated and basilar papillae dissected out, incubated in low-Ca^{2+} saline (Table 1) containing protease (0·03 mg ml^{-1}, Sigma P8038), and the tectorial membrane removed. Next, the papillae were incubated in low-Ca^{2+} saline to which papain (Calbiochem, 0·36 mg ml^{-1}), L-cysteine (0·44 mg ml^{-1}) and bovine serum albumin (BSA fraction V; 0·1 mg ml^{-1}) were added. This solution was exchanged for low-Ca^{2+} saline containing DNase I (Type IV, 0·02 mg ml^{-1}) and BSA (0·2 mg ml^{-1}) before hair cells were harvested and transferred to a glass recording chamber filled with either normal saline (Table 1) or saline supplemented with BSA (0·4 mg ml^{-1}). Cells were observed using Nomarski-DIC optics on an inverted microscope (Zeiss IM). Electrical recordings were performed at 22–24 °C for up to 5 h after decapitation.

In some experiments, attachments between hair cells and supporting cells were loosened without the use of papain. Instead, basilar papillae were perfused with an EDTA-buffered saline having ~30 μM free Ca^{2+} and ~5 mM free Mg^{2+} (Table 1) for a period of 30–40 min. Hair cells were collected and plated as described above. This method was useful for a narrow range of free Ca^{2+} concentrations: the kinocillium separated from the hair bundle if free Ca^{2+} was less than about 20 μM, and the yield of hair cells was greatly reduced if free Ca^{2+} was greater than about 60 μM. Free Ca^{2+} was measured with a Ca^{2+}-selective electrode (Microelectrodes, Inc., Bedford, NH, USA) and adjusted to ~30 μM using EDTA (0·1 M) or $CaCl_2$ (1 M), as needed. Hair cells isolated without papain had similar electrical properties, apart from an improved responsiveness to exogenous acetylcholine (M. B. Goodman & J. J. Art, unpublished observations). In particular, both methods produced hair cells that exhibited electrical resonance near −50 mV and over an identical range of resonant frequencies (Fig. 1*E*). Therefore, the results are reported without regard to the isolation procedure used.

Recording pipettes were pulled from soda-glass capillaries (resistances, 1–3 MΩ; tip diameter, ~1 μm), coated with Sylgard® 182 and fire-polished immediately before use. Unless otherwise stated, the patch electrode was filled with a K^+-based solution containing (mM): KCl, 125; $MgCl_2$, 2·8; $CaCl_2$, 0·45; K_2EGTA, 5; Na_2ATP, 2·5; K-Hepes, 5. Membrane current and voltage were recorded using standard whole-cell patch clamp methods with a modified Yale Mark V amplifier (Art & Fettiplace, 1987). Experiments were recorded on videotape by an 8-channel PCM unit (VR-100; Instrutech, Great Neck, NY, USA) and analysed off-line. To avoid jitter, the clock circuit of the PCM was used to control voltage and current clamp commands and digitization. The data were filtered at 3·2 kHz (8-pole Bessel filter) and digitized at up to 24 kHz.

Membrane voltages were corrected for liquid junction potentials and errors due to current flow across uncompensated series resistance, which lay between 1 and 6 MΩ. To measure whole-cell capacitance and series resistance, each cell was voltage clamped at −70 mV and stepped to −65 mV for 6 ms. The resulting time-dependent current was assumed to flow across the cell's capacitance and series resistance. Leak conductance and capacity transients were measured from the current evoked by ±5 mV pulses from −75 mV in the presence of external Cs^+ (5 mM) to block current carried by a K^+-selective inward rectifier (Goodman & Art, 1996). Except where noted, leakage currents and capacity transients have been subtracted from the illustrated records. All data were analysed and plotted using Igor Pro 2 (WaveMetrics, Lake Oswego, OR, USA). A Levenberg–Marquardt, non-linear least-squares minimization algorithm was used in the curve-fitting routines (Press, Teukolsky, Vetterline & Flannery, 1994). Values for n observations are reported as mean ± standard deviation.

Table 1. Composition of external solutions (mM)

	NaCl	KCl	$CaCl_2$	$MgCl_2$	Hepes	EDTA
Normal	125	4	2·2	2·8	10	—
TEA (x = [TEA])	130 − x	4	2·2	2·8	5	—
4-AP (x = [4-AP])	130 − x	4	2·2	2·8	5	—
Reduced Ca^{2+}	125	4	0·1	2·8	10	—
Buffered Ca^{2+}	110	4	1·5	8·5	5	5

Solutions adjusted to pH 7·6 with NaOH. Glucose (0·8 mM) was added to each solution before use.

Solutions

Extracellular solutions were based on normal turtle saline (Table 1). Drugs applied in excess of 1 mM were substituted for an equimolar concentration of NaCl. The cell's response reflects the action of the added drug since neither complete replacement of Na^+ with *N*-methylglucamine nor partial replacement of Cl^- with methanesulphate had any effect on the whole-cell current. Tetraethylammonium (TEA) was obtained as TEA-OH (Aldrich Chemical, Milwaukee, WI, USA) and titrated with HCl to yield a 1 M stock solution. 4-Aminopyridine (4-AP) was diluted from a 30 or 60 mM stock solution, prepared daily from solid. After dilution, the pH was adjusted to 7·6 with HCl. A calibrated stock solution (1 M) of $CaCl_2$ was purchased from BDH through their US distributor (Gallard-Schlesinger). Puratronic grade $MgCl_2$ was purchased from Alfa Chemical (Ward Hill, MA, USA). All other reagents were obtained from Sigma.

Solution exchange

Rapid, local solution exchange was achieved using methods described previously (Art *et al.* 1993). External solutions were applied using two 6-barrelled 'pan-pipes' (Vitro Dynamics, Rockaway, NJ, USA) positioned at angles of 180 and 225 deg with respect to the recording electrode, and removed by a U-tube positioned at 270 deg. Each barrel had an internal cross-section of 75 μm and was perfused by means of a remote-controlled miniature solenoid valve (The Lee Co., Westbrook, CT, USA). Normal saline solution was supplied from the barrel located furthest from the U-tube, while the most concentrated drug solution was supplied from the barrel closest to the U-tube.

Measuring resonant frequency

Resonant frequency (f_0) and quality (Q_{3dB}) were measured either from damped voltage oscillations elicited by a step of injected current (Fig. 1*C*) as described (Art & Fettiplace, 1987) or from the spectrum of steady voltage oscillations, which were often apparent near the zero-current potential (Fig. 1*A*). In some cells, a modest holding current (<100 pA) was used to maintain the membrane potential near −50 mV. Relative spectral density (RSD) was estimated from long stretches (5–10 s) of voltage oscillations using the method of modified periodograms (see pp. 414–419 of Rabiner & Gold, 1975). Briefly, voltage oscillations were expressed relative to the mean membrane potential and divided into five to ten overlapping segments of size w (in sample points). Segment size was a power of two and chosen to maximize frequency resolution which lay between 0·7 and 2 Hz and was determined by $1/(w\Delta t)$ where Δt is the digitization sample interval. The total bandwidth contained in the RSD is given by $1/(2\Delta t)$ and was at least 2 kHz. To compute the RSD curves shown in Fig. 1*B*, segments were multiplied by a Hamming window, transformed to the frequency domain by fast Fourier transform, and a segment RSD was computed from the sum of the squares of the real and imaginary parts. Individual segment RSDs were averaged to yield the curves shown in Fig. 1*B*. This method provides computational efficiency, good frequency resolution and minimizes spectral leakage and random noise. Resonant frequency was determined from the frequency of maximum spectral density, and Q_{3dB} was calculated from f_0 divided by the half-power bandwidth.

Resonant frequency (Fig. 1*C*) is related to the time constant, τ, of membrane current relaxation at −50 mV (Fig. 1*D*) according to (Art & Fettiplace, 1987; Wu *et al.* 1995):

$$f_0 = k_1\tau^{-\frac{1}{2}} + k_2. \quad (1)$$

The coefficients k_1 and k_2 were determined empirically by plotting the frequency that gave the highest Q_{3dB} in each cell against τ. Cells isolated using papain and buffered Ca^{2+} saline solutions spanned the same range of resonant frequencies, and their results have been pooled to obtain the best possible estimate of the coefficients k_1 and k_2 (Fig. 1*E*). Equation (1) was used to estimate resonant frequency from voltage clamp records and the result indicated as $\hat{f}_0$.

RESULTS

The ionic selectivity of outward current

Previous attempts to establish the ionic basis of outward current in hair cells have indicated that tail currents in low frequency cells reverse polarity near the K^+ equilibrium potential (Art & Fettiplace, 1987) and that instantaneous current–voltage relations in high frequency cells display an outward rectification that interferes with accurate measurement of a reversal potential (Art & Fettiplace, 1987; Fuchs & Evans, 1990). We reasoned that measurement of inward current in high frequency cells was compromised by the increasing rate of deactivation observed with hyperpolarization and the limited bandwidth of whole-cell recording (Art & Fettiplace, 1987). This was tested by measuring tail current reversal in the presence of elevated external K^+ (20 mM), a manoeuvre which shifts the K^+ equilibrium potential to −48 mV. Outward current was activated by a step to −20 mV followed by repolarization to voltages between −120 and −30 mV. Results from a cell whose $\hat{f}_0$ was 270 Hz are shown in Fig. 2. In nine cells, the reversal potential had a mean value of −47·8 ± 3·0 mV (n = 9) and showed no systematic relation to $\hat{f}_0$. In three low frequency cells with tail currents slow enough to measure at potentials negative to −90 mV, the reversal potential had a mean value of −84·8 ± 4·7 mV (n = 3) in

normal (4 mM K^+) saline. These values agree with those expected of a pure K^+ conductance with predicted reversal potentials in 4 and 20 mM external K^+ of −86 and −48 mV, respectively, indicating that outward current is carried chiefly by K^+ ions in all hair cells.

Potassium current pharmacology

Single-cell dose–response relations were measured in cells tuned to different frequencies and used to discover if outward current was carried by one or more K^+ channel types. The sensitivities to K^+ channel antagonists TEA and 4-AP were also used to classify hair cell K^+ channel types. Cells were held at −60 mV and blockade of outward current was tested during voltage pulses to −40 mV. To compute dose–response relations it was necessary to devise a method for isolating K^+ current, since the measured current represents a sum of an outward K^+ current and inward Ca^{2+} current (Lewis & Hudspeth, 1983; Art & Fettiplace, 1987). This was accomplished either by subtracting inward current revealed in the presence of large antagonist concentrations from the net current or by measuring K^+ current amplitude from the tail current amplitude recorded upon repolarization. Tail current amplitude was measured by fitting the decay of outward current with an exponential function and using the fitted function to calculate the current flowing at the time of repolarization. Half-blocking concentrations determined

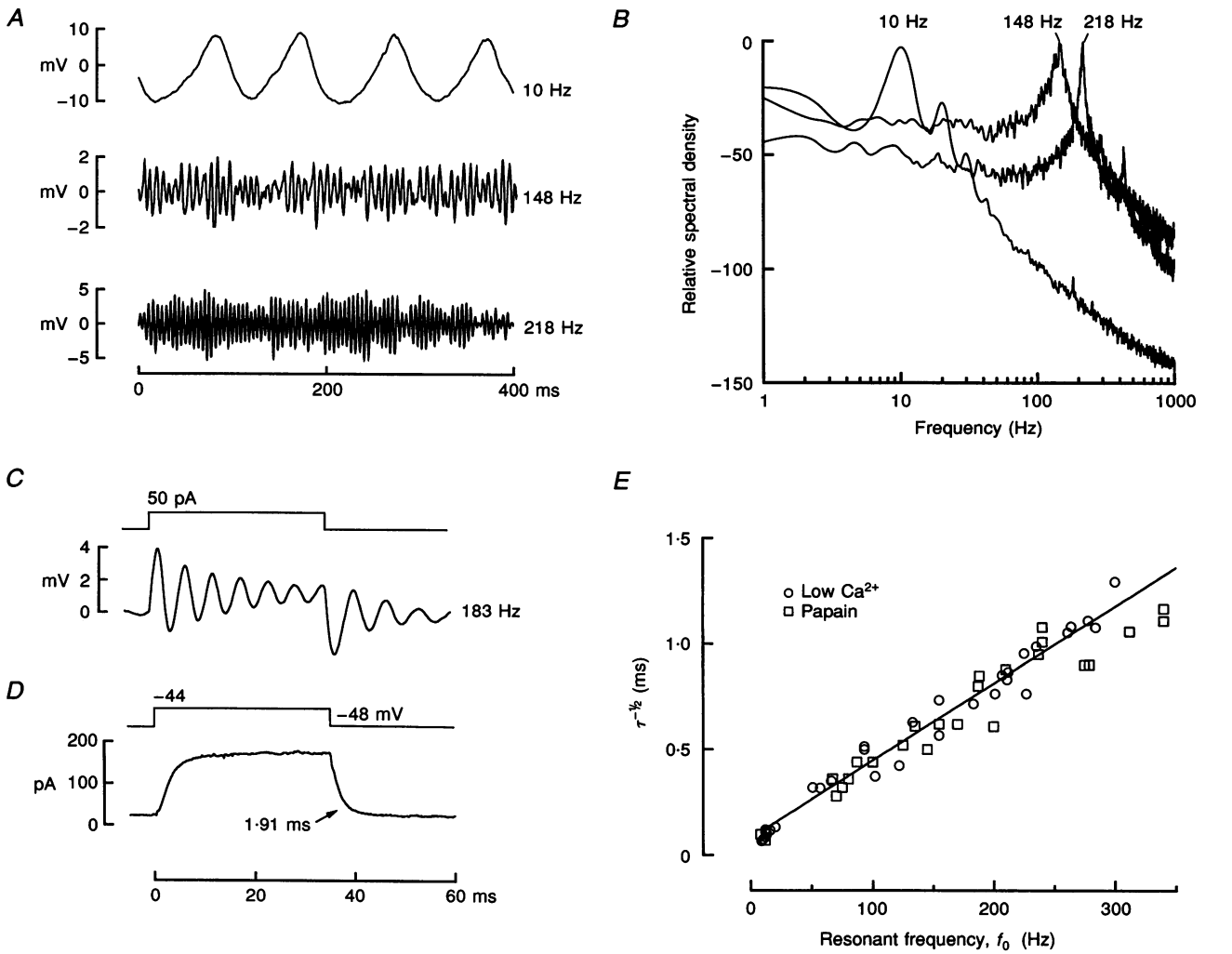

Figure 1. Measuring resonant frequency

A, steady, sinusoidal oscillations in membrane potential were recorded from cells in current clamp. Ordinates are expressed relative to the mean membrane potential recorded in each cell. Mean potential and injected current were (top to bottom): −48 mV, 70 pA; −52 mV, 0 pA; −44 mV, 0 pA. *B*, relative spectral density computed from 5–10 s segments of steady oscillations, expressed in dB relative to the maximum. Same cells as in *A*. Resonant frequency, Q_{3dB}, and ordinate scaling factors were: 10 Hz, 6, 25·4 mV^2 Hz^{-1}; 148 Hz, 39, 0·0351 mV^2 Hz^{-1}; 218 Hz, 51, 0·238 mV^2 Hz^{-1}. *C*, damped oscillations elicited by a +50 pA current step. Voltage is expressed relative to the mean resting potential, −48 mV. *D*, current elicited by a +4 mV step from the mean resting voltage, same cell as in *C*. *E*, time constant of current decay is correlated with f_0. ○, buffered calcium isolation; □, papain isolation. Smooth line fitted to data with a slope of 0·00376 and a linear correlation coefficient, *R*, of 0·99 for $n = 62$.

from steady-state and tail currents were similar in cells in which a direct comparison was possible. Depolarizing pulses were interleaved with steps to −120 mV so that blockade of inward current carried by a K^+-selective inward rectifier was monitored concurrently.

Inhibition of outward current by external TEA

Figure 3*A* shows dose-dependent block of outward current by external TEA in a cell with a value for f_0 of 93 Hz. Ten concentrations, exponentially distributed between 50 μM and 130 mM TEA, were applied to maximize resolution of possible multiple binding sites. Concentrations in excess of 2·5 mM reveal an inward current carried by Ca^{2+} ions, as shown previously (Art & Fettiplace, 1987). Total K^+ current was computed by subtracting inward current recorded in isotonic TEA (130 mM), plotted against TEA concentration, and fitted with a single-site, equilibrium binding curve,

$$I_K = I_0 (K_i/(K_i + x)), \quad (2)$$

where I_0 is K^+ current recorded in normal saline, x is TEA concentration, and K_i is the concentration required for half-block (Fig. 3*C*). We confirmed the apparent binding stoichiometry by fitting the data with a Hill equation. In this experiment and those described below, the Hill coefficient determined by this procedure was within 4% of 1, indicating that a single molecule binds each channel. A second cell tuned to 259 Hz gave similar results. These results were normalized by plotting the fractional inhibition, I/I_0, as a function of external TEA concentration. The pooled data are consistent with a half-blocking concentration of 0·215 mM (open symbols, Fig. 3*C*).

Outward current in lower frequency cells (<30 Hz) was less sensitive to inhibition by external TEA and even isotonic TEA failed to reveal an inward I_{Ca} during depolarization (Fig. 3*B*). In these cells, K^+ current was separated from Ca^{2+} current by using tail current amplitude to measure the K^+ current. This separation relies on the fact that I_{Ca} does not significantly contribute to the tail current because it deactivates with a time constant of ~150 μs at −60 mV (Art & Fettiplace, 1987). Single-cell dose–response curves were constructed by plotting K^+ current amplitude against TEA concentration in four cells with estimated resonant frequencies between 10 and 20 Hz. In all cases, the dose–response curve was described by a single class of binding sites with a 1:1 stoichiometry. The half-blocking concentration showed no significant variation with f_0 and had a mean value of 35·9 ± 2·2 mM ($n = 4$). The collected results in high and low f_0 cells are shown in Fig. 3*C*, normalized to K^+ current in normal saline. While the main effect of TEA was a reduction in K^+ current amplitude, we tested if TEA modified K^+ kinetics or revealed a current with distinct kinetics by comparing normalized K^+ current traces in control and 25 mM TEA saline (Fig. 3*B*, inset). Their superposition demonstrates that TEA reduces K^+ current amplitude without affecting kinetics.

Figure 3*C* shows that the apparent TEA affinity of the channels carrying outward current in low f_0 cells is nearly 200-fold lower than in high f_0 cells, a result which argues that outward current is carried by a distinct class of K^+ channels in cells tuned to the lowest frequencies compared with cells tuned to more than 90 Hz. High affinity for TEA is characteristic of large-conductance Ca^{2+}-activated K^+ channels (Yellen, 1984) and is consistent with earlier evidence for BK channels in hair cells (Art & Fettiplace, 1987; Hudspeth & Lewis, 1988; Art, Wu & Fettiplace, 1995). A low affinity for TEA in low f_0 cells may indicate the existence of a purely voltage-gated K^+ current, $I_{K(V)}$. Additional support for this conclusion comes from the observation that outward current persists in low frequency cells when extracellular Ca^{2+} is reduced below 0·1 μM (Art *et*

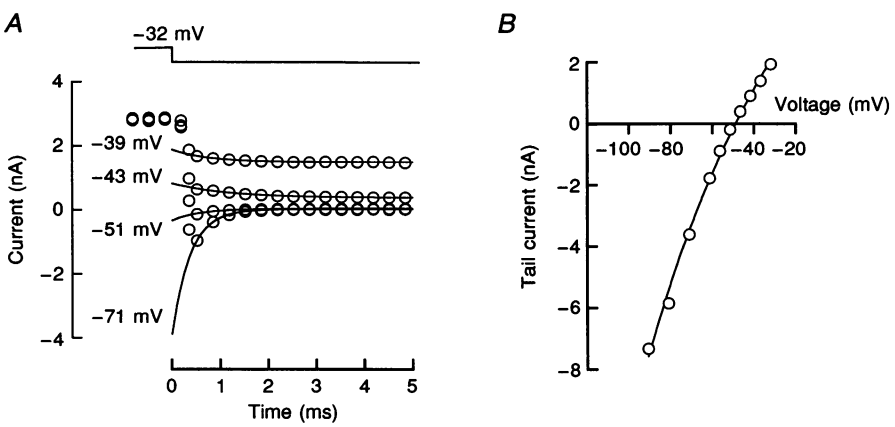

Figure 2. Tail currents recorded in 20 mM external K^+

A, tail currents in a cell tuned to 270 Hz. Outward current was activated by a 40 ms voltage step to −32 mV and repolarized to the voltages indicated to the left of each plot. Tail current records (○) were fitted by a single exponential function (continuous lines) and reversed polarity by −51 mV. *B*, instantaneous current found from exponential fits to tail current relaxations in *A*, plotted against membrane voltage. Current exhibits a mild inward rectification and reversed polarity at −49 mV.

al. 1993). The role of intracellular Ca^{2+} in gating outward current was also tested using an intracellular solution containing 30 mM BAPTA (data not shown). Although this increases buffering capacity and speed, it fails to block outward current in low f_0 cells. In addition, patches excised from low frequency cells frequently contain a voltage-gated K^+ channel whose ensemble-average current has decay constants appropriate for low frequency resonance (Art *et al.* 1995).

Inhibition of outward current by 4-AP

4-AP is frequently used to inhibit voltage-gated K^+ channels and was used to characterize further outward current in low f_0 cells. Unlike external TEA, 4-AP has access to both sides of the plasma membrane because it exists primarily as an uncharged, hydrophobic molecule at physiological pH (7·6). It is likely to bind to a site on the internal face of K^+ channels, as originally demonstrated for voltage-gated K^+ current in squid axon (Kirsch & Narahashi, 1983). In low f_0

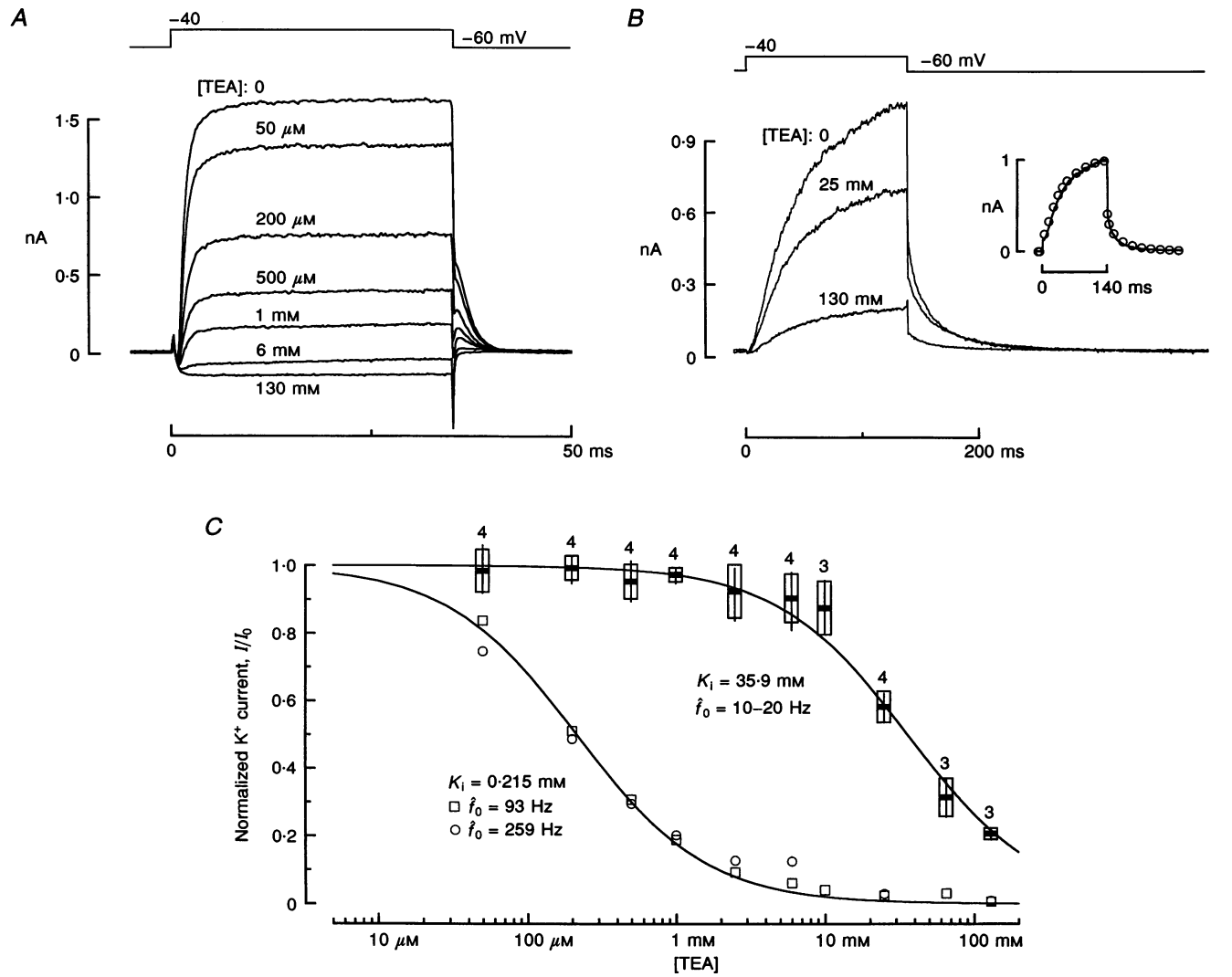

Figure 3. The effect of external TEA on outward current in cells of high and low frequency

A, inhibition of net current in a 93 Hz cell. Each trace is a leak-subtracted average of 5–10 presentations. *B*, inhibition of net current in a low frequency cell (18 Hz). Each trace is a leak-subtracted average of 3–5 presentations. Inset, normalized K^+ current recorded in normal and 25 mM TEA salines. Inward current estimated from the ratio of K^+ to Ca^{2+} current determined previously (Art *et al.* 1993) was subtracted from the net current in *B* to obtain the total K^+ current. Continuous trace, normal saline; ○, K^+ current in 25 mM TEA. For clarity, not all data points are displayed. *C*, comparison of TEA inhibition in high and low frequency cells. Potassium current was normalized to I_0 in two high frequency cells with values for f_0 of 93 Hz (□) and 259 Hz (○). Horizontal bars show mean normalized inhibition by TEA recorded in four low f_0 cells (10–20 Hz), boxes extend for a standard deviation, and vertical lines indicate the range of values recorded in all cells tested. The number of cells tested at each dose is indicated on the graph. Dose–response curves were fitted using eqn (2) by setting I_0 to 1 and yielded affinities of 0·215 and 35·9 mM for high and low frequency cells, respectively.

hair cells, 4-AP blockade increases with repeated activation of outward current and was allowed to reach a steady level at each concentration tested. For concentrations less than 1 mM 4-AP, inhibition could be relieved by a combination of superfusion with normal saline and repeated depolarization. Above 1 mM 4-AP, outward current was only partly restored within 2 min by this procedure. The recovery may have been slowed by the need to remove 4-AP from the internal as well as the external environment.

Single-cell dose–response experiments were identical to those described for TEA. In six cells with f_0 between 24 and 6 Hz, half-blocking concentrations for 4-AP lay between 26 and 102 μM. Results for one cell with $K_i = 70$ μM are shown in Fig. 4*A*. Current followed a similar time course in 4-AP

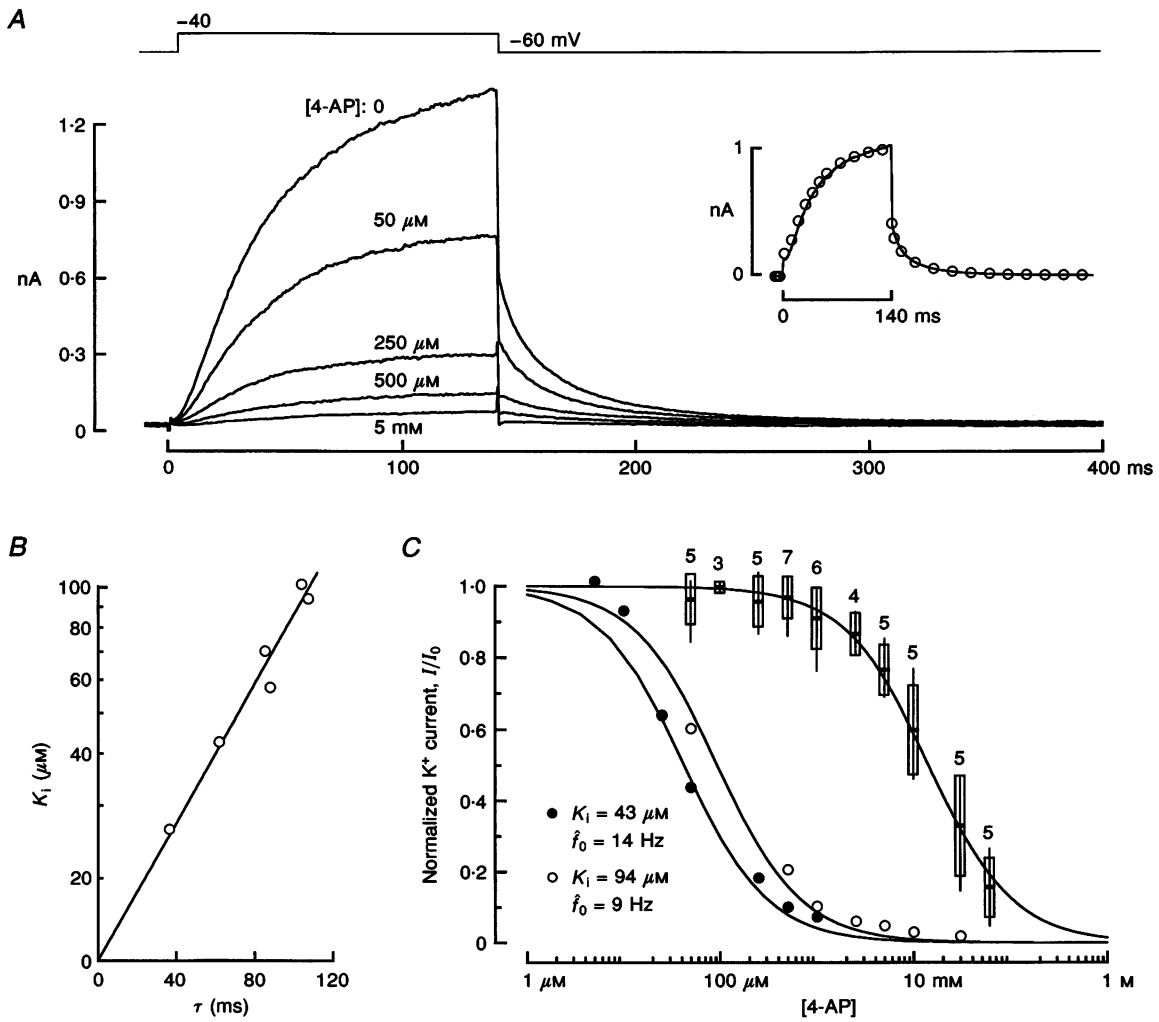

Figure 4. The effect of 4-AP on outward current

A, inhibition of net current. Each trace is a leak-subtracted average of 3–5 presentations, after inhibition reached a steady level in each solution. $f_0 = 6$ Hz. Inset, K^+ current in normal and 50 μM 4-AP salines, normalized with respect to the K^+ current amplitude in the last 50 ms of a 140 ms voltage step. To obtain the total K^+ current, inward current was estimated as described for Fig. 3*B* and subtracted from the traces in *A*. Continuous trace, normal saline; ○, K^+ current in 50 μM 4-AP. For clarity, not all points were displayed. *B*, half-blocking dose, K_i, for 4-AP *versus* time constant of current decay at −50 mV, τ. A high affinity site for inhibition by 4-AP was measured in single-cell dose–response experiments in 6 cells with f_0 between 6 and 24 Hz. The half-blocking dose increases exponentially with τ according to $K_i = 12{\cdot}6\exp(\tau/52{\cdot}1)$. *C*, inhibition by 4-AP in cells of low and high resonant frequency. Potassium current was normalized to I_0 and measured either from tail current amplitude or steady-state current. ●, inhibition by 4-AP in a cell with $f_0 = 14$ Hz fitted by eqn (2) with $K_i = 43$ μM. ○, results in a second cell with $f_0 = 9$ Hz and $K_i = 94$ μM. Horizontal bars show mean inhibition by 4-AP recorded in seven high f_0 cells (179–296 Hz), boxes indicate the standard deviation, and vertical lines indicate the range of values recorded in all cells tested. The number of measurements at each dose are given above each point. The relation between K^+ current amplitude and 4-AP concentration was fitted by eqn (2) with $I_0 = 1$ and $K_i = 14{\cdot}3$ mM.

(Fig. 4A, inset), indicating that 4-AP did not alter its kinetics. Dose–response curves for two other cells are shown in Fig. 4C. As illustrated in Fig. 4B, apparent affinity constants were correlated with the time constant of current decay at −50 mV and, hence, resonant frequency. This systematic variation in 4-AP affinity may provide a clue for understanding variation in K^+ current kinetics, at least in low f_0 cells. While the mechanism linking 4-AP affinity to kinetics is unknown, it is worth noting that a similar correlation has been described in cloned K^+ channels (Kirsch & Drewe, 1993) and that small changes in the amino acid residues flanking the interior of the putative pore region are sufficient to modulate deactivation rate and 4-AP affinity in tandem (Shieh & Kirsch, 1994).

Potassium current in high f_0 cells was inhibited by concentrations of 4-AP greater than about 1 mM. A single-cell dose–response relation in a 296 Hz cell was consistent with a single class of low-affinity binding sites having 1:1 stoichiometry for 4-AP (K_i = 13·8 mM). In this cell, 4-AP did not affect the time course of K^+ current activation (not shown). Similar results were obtained in two additional cells; results from all three cells were normalized to K^+ current amplitude measured in normal saline, combined with partial dose–response curves from four additional cells and used to determine K_i (Fig. 4C). 4-AP block in two other high f_0 cells gave slightly lower affinity, modified K^+ current kinetics and was best fitted with a Hill coefficient of approximately 1·4. While the reason for this departure from 1:1 stoichiometry is unknown, it suggests that inhibition of the BK channel by 4-AP is a complex process. Nevertheless, these results indicate that even in the worst case the BK channel current is 100-fold less sensitive to 4-AP than is the K^+ current in low f_0 cells (Fig. 4C). Several intermediate f_0 cells had dose–response relations consistent with at least two classes of binding sites, suggesting that some hair cells contain a mixture of K^+ currents.

Inhibition of inward K^+ current by TEA and 4-AP

We also tested the effect of TEA and 4-AP on inward current carried by the K^+-selective inward rectifier, $I_{K(IR)}$. These data are required in order to interpret the effects of these agents on electrical resonance (see Fig. 7), since other agents that block $I_{K(IR)}$, such as external Cs^+, decrease resonant quality (Goodman & Art, 1996). The experiment consisted of voltage steps to −120 mV where inward current is primarily $I_{K(IR)}$, interleaved with depolarizing steps so that inhibition was examined in the same cells used to ascertain outward current pharmacology. Apart from variations in amplitude, $I_{K(IR)}$ was similar in all cells. Accordingly, results were pooled without regard to resonant frequency; cells with f_0 between 3 and 245 Hz were tested. Inhibition by 4-AP was consistent with a single binding site with 1:1 stoichiometry and an apparent dissociation constant of at least 90 mM (n = 6). An inhibition curve for TEA was compiled from measurements in four cells and was best described by two classes of binding sites with half-blocking concentrations of K_1 = 3·9 mM and K_2 = 160 mM. The reason for two apparent binding sites is unknown; the higher affinity site may reflect inhibition of inward current carried by voltage-independent Ca^{2+}-activated K^+ channels, SK channels, that are half-blocked by ~5 mM TEA (Tucker & Fettiplace, 1996), while the lower affinity site is likely to represent TEA blockade of $I_{K(IR)}$.

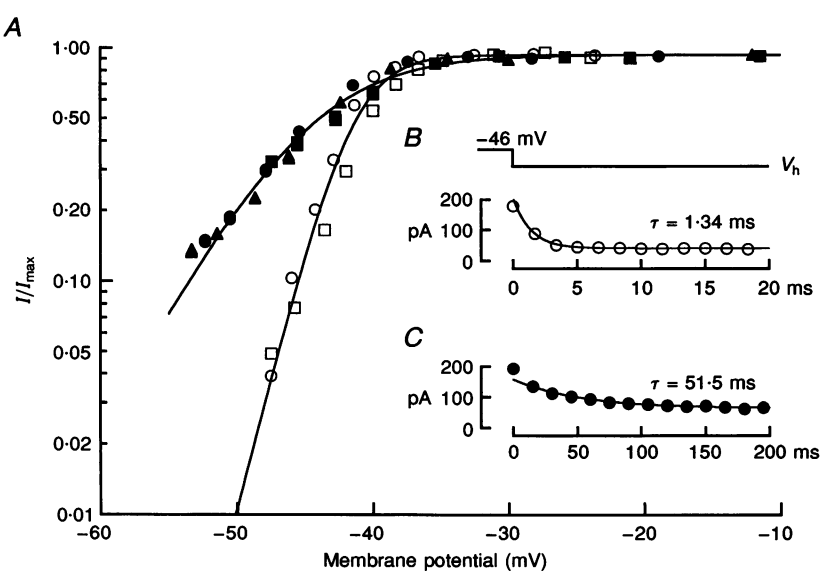

Figure 5. Steady-state voltage dependence of activation

A, $I_{K(Ca)}$ was isolated by superfusing cells with 0·8 mM 4-AP and increased e-fold in 1·9 mV (open symbols); $I_{K(V)}$ was isolated by superfusing cells with 25 mM TEA and increased e-fold in 4·0 mV (filled symbols). Different symbols correspond to different cells. *B*, relaxation of $I_{K(Ca)}$ following a 4 mV depolarization. Deactivation was fitted by a single exponential function with a time constant of 1·34 ms. *C*, relaxation of $I_{K(V)}$ fitted by a single exponential function with a time constant of 51·5 ms.

Sensitivity of Ca^{2+} current to TEA and 4-AP

Thus far, we have assumed that TEA and 4-AP exert their effect on membrane current in hair cells by binding directly to K^+ channels. However, inhibition of $I_{K(Ca)}$ could arise from an effect on the voltage-dependent Ca^{2+} current. This possibility was explored by testing their effects on Ca^{2+} current, isolated by replacing K^+ with Cs^+ in the internal solution. To maximize Ca^{2+} current amplitude, the external solution contained 5 mM Ca^{2+} as the only divalent cation. Under these conditions, 65 mM TEA does not significantly affect peak Ca^{2+} current, confirming our assumption that inhibition of $I_{K(Ca)}$ by TEA is a direct effect. In contrast, 10 mM 4-AP blocked approximately 15% of peak inward Ca^{2+} current, a result which may account for the larger Hill coefficient required to produce an adequate fit of 4-AP inhibition curves in some high f_0 cells. Inhibition of Ca^{2+} current by 4-AP is unlikely to affect inhibition curves in low f_0 cells since outward current blockade is nearly complete at 1 mM, a concentration which inhibits peak Ca^{2+} current by only ~4%.

Steady-state voltage dependence

Potassium channel types may be considered distinct if they differ in several of the following attributes: pharmacology, single-channel amplitude, voltage dependence and kinetics. Membrane patches excised from low and high frequency hair cells contain channels with mean conductances of 45 and 322 pS in symmetrical 150 mM K^+, respectively (Art *et al.* 1995). A similar distribution of low and high conductance channels was inferred from whole-cell current noise in the chick cochlea (Fuchs & Evans, 1990). Here, we have shown that outward K^+ current in low f_0 cells is pharmacologically distinct from outward K^+ current in high f_0 cells (summarized in Table 2). This differential sensitivity was exploited to isolate each K^+ current type and to compare their voltage dependence of activation. Steady-state activation curves were constructed from the tail current amplitude on repolarization to about −50 mV recorded in the presence of either 25 mM TEA or 0·8 mM 4-AP to isolate $I_{K(V)}$ and $I_{K(Ca)}$, respectively. Voltage dependence was quantified by normalizing the tail current amplitude and fitting the steady-state activation curve with a Boltzmann function:

$$I/I_{max} = 1/\{1 + \exp((V - V_0)/V_e)\}. \quad (3)$$

where I/I_{max} is the relative current, V_0 is the mid-point of activation and V_e is a slope factor. Results for three low f_0 and two high f_0 cells are shown in Fig. 5. To examine $I_{K(V)}$ in isolation, activation curves in low f_0 cells were collected in the presence of 25 mM TEA (Fig. 5*A*, filled symbols). This concentration is sufficient to inhibit 99% of current carried by $I_{K(Ca)}$ and 40% of $I_{K(V)}$ (see Table 2). Current increases e-fold in 4·0 ± 0·3 mV ($n = 3$), reaches its half-maximum at −44·3 ± 0·8 mV ($n = 3$), and exhibits the resistance to external TEA characteristic of a purely voltage-gated K^+ current. Similarly, $I_{K(Ca)}$ was examined in isolation by measuring steady-state activation in the presence of sufficient 4-AP (0·8 mM) to block ~90% of any K_V channels that might be present (Fig. 5*A*, open symbols). Normalized tail current was half-maximal at −41·3 mV and increased e-fold in 1·9 mV ($n = 2$). The steep voltage dependence is likely to result from the combined effect of membrane voltage and voltage-dependent elevation of intracellular Ca^{2+} on gating BK channels and agrees well with previous results in high frequency hair cells (Art *et al.* 1995).

Table 2. Apparent dissociation constants, K_i (mM)

Drug	K^+ channel type		
	K_V	BK	K_{IR}
External TEA	35·9	0·215	3·6; ⩾160
4-AP	0·026–0·102	12·3	⩾93

Apparent dissociation constants measured from single-cell dose–response relations for inhibition by TEA and 4-AP. Values for K_V channels represent the mean value measured in 4–6 cells having f_0 less than 30 Hz, while values for BK channels are the mean of measurements in two cells with f_0 greater than 93 Hz. Values for K_{IR} channels were pooled from 4 cells in each group, having f_0 between 3 and 245 Hz.

Inactivation of 4-AP-sensitive current

Potassium currents in hair cells have been separated into an adapting or A-type current and a sustained current ascribed either to a Ca^{2+}-activated K^+ current (Lewis & Hudspeth, 1983; Hudspeth & Lewis, 1988) or a purely voltage-gated, sustained K^+ current (Housley *et al.* 1989; Rennie & Ashmore, 1991; Murrow, 1994). While the voltage-gated K^+ current of turtle hair cells is stable during brief (100–200 ms) depolarizing voltage pulses, it declines to a steady level during maintained depolarization (9 s). The voltage-gated current was isolated using 25 mM TEA to inhibit $I_{K(Ca)}$ (Control in Fig. 6*A*), as in experiments that measured the voltage dependence of activation (see Fig. 5). Addition of 0·8 mM 4-AP blocked similar fractions of peak and steady current (4-AP in Fig. 6*A*), suggesting that both components are carried by a single class of K^+ channels. The difference between these traces gives the current carried by $I_{K(V)}$ (Difference in Fig. 6*A*) since it is the only current affected by this concentration of 4-AP. The difference trace in Fig. 6*A* shows that $I_{K(V)}$ reaches a steady level equal to nearly half of the peak current at the end of a 9 s voltage step, suggesting that it can be regarded as a partially adapting current. During depolarization to more than −30 mV, $I_{K(V)}$ relaxes in two phases having time constants of 117 and 1230 ms. Incomplete inactivation with a similar time course has been observed in saccular hair cells (Sugihara & Furukawa, 1995) and a mammalian cell line stably transfected with human Kv1·5 (Snyders, Tamkun & Bennett, 1993).

The voltage dependence of steady-state inactivation was assessed by holding the membrane voltage at a series of

values between −90 and −30 mV for a period of 11 s (V_c) and measuring peak current during a brief (140 ms) test pulse to −20 mV (Fig. 6*B*). Cells were then repolarized to −90 mV for at least 9 s, this interval being ~3-fold longer than the time constant for recovery from inactivation as measured by a paired-pulse experiment. Test current was normalized to peak current recorded after holding the cell at −90 mV (Fig. 6*C*, ●) and declined to approximately 0·3 at −30 mV. The relative current, I/I_{max}, declined with depolarization to R_{min}. The relation between inactivation and voltage was fitted by a modified Boltzmann function:

$$I/I_{max} = R_{min} + (1 - R_{min})/(1 + \exp((V - V_0)/V_e)), \quad (4)$$

where V_0 is the voltage at which I/I_{max} is equal to $(R_{min} + 1)/2$.

As shown in Fig. 6*C*, activation (○) and inactivation (●) occur over the same voltage range. Similar results were obtained in nine cells and the voltage dependence of inactivation was fitted by eqn (4). In all cells examined, inactivation was incomplete and R_{min} varied between 0·28 and 0·5 with a mean value of 0·39 ± 0·07 ($n = 9$). Mean values for V_0 and V_e were −50 ± 6 mV and 3·0 ± 0·6 mV, respectively. Despite its slow onset, inactivation may prove to be an important determinant of the behaviour of $I_{K(V)}$ since it occurs over the same voltage range as activation. Preliminary efforts to examine the behaviour of $I_{K(V)}$ have indicated that, in some cells tuned to low frequencies, deactivation is best described by a sum of two exponential decay functions (Goodman, 1995). A slower component is explained by inactivation if a fraction of K_V channels are inactivated during brief depolarizations and these channels must re-enter the open state before closing. The macroscopic behaviour of $I_{K(V)}$ will be documented in detail elsewhere. For current purposes, the faster time constant was used to estimate resonant frequency in all cells showing evidence for multiple components of current decay at −50 mV.

Sensitivity of electrical resonance to TEA and 4-AP

Outward current in hair cells tuned to low frequencies (<30 Hz) is pharmacologically distinct from outward current in cells tuned to higher frequencies. Figure 7 shows electrical resonance in low and high frequency cells exposed to normal saline, TEA and 4-AP. The choice of antagonist concentration was guided by the apparent affinities measured in single-cell dose–response experiments (Table 2) and chosen to preferentially inhibit either $I_{K(Ca)}$ or $I_{K(V)}$. The concentration and percentage inhibition of $I_{K(Ca)}$ and $I_{K(V)}$ were 6 mM, 96% $I_{K(Ca)}$ and 14% $I_{K(V)}$ for TEA, and

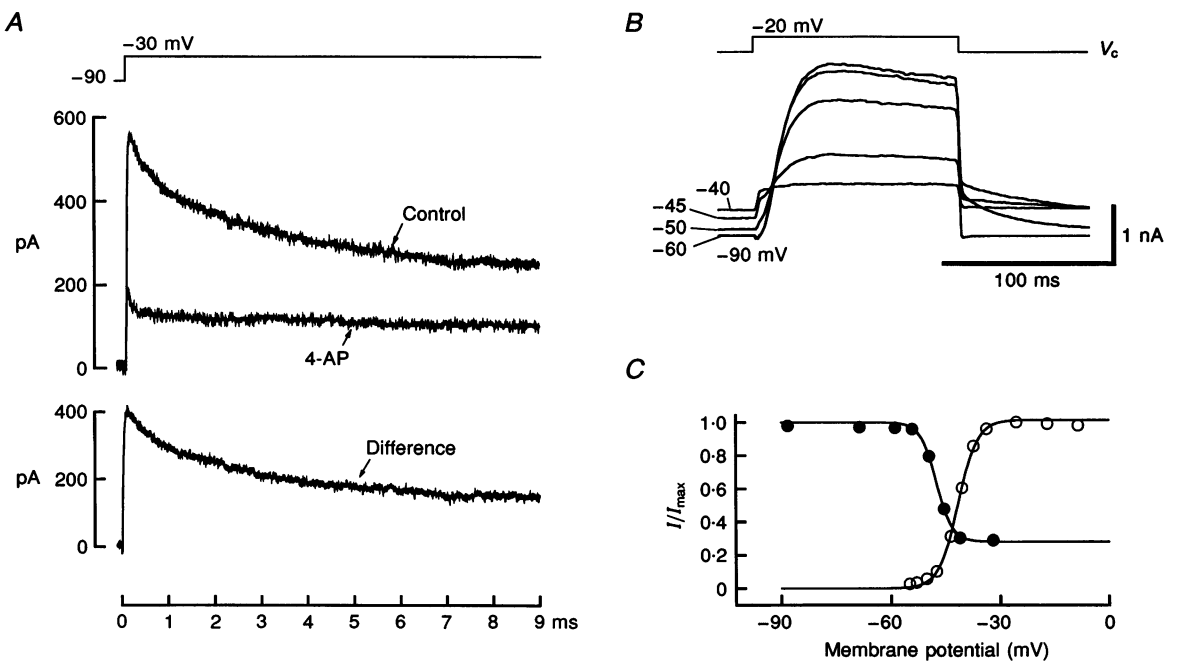

Figure 6. Transient and maintained current carried by K_V channels

A, membrane current carried in 25 mM TEA alone (Control) and in 25 mM TEA and 0·8 mM 4-AP (4-AP). Membrane potential was held at −90 mV and stepped to −30 mV for 9 s every 60 s. The 4-AP-sensitive current (Difference) reaches a peak within 50 ms and decays to a steady level after 9 s depolarization. Total current includes a leak component. *B*, superimposed traces recorded in the presence of 25 mM TEA for a test pulse to −20 mV following 11 s at the conditioning voltage (V_c) indicated. The cell was voltage-clamped at −90 mV between conditioning pulses. *C*, voltage dependence of inactivation. Peak current at −20 mV was measured from the traces in *B*, expressed relative to the value recorded following a conditioning interval at −90 mV and plotted against the conditioning voltage (●). The voltage dependence of activation was measured in the same cell from tail current amplitude on repolarization to −50 mV, normalized to its maximum (○).

0·8 mM, 5% $I_{K(Ca)}$ and >90% $I_{K(V)}$ for 4-AP. It is important to note that these concentrations of TEA and 4-AP do not significantly affect either Ca^{2+} current or the K^+-selective inward rectifier (see above). In a low frequency cell (Fig. 7*A*), TEA had no detectable effect on the mean membrane potential, f_0, or Q_{3dB}. Slow voltage oscillations in chick cochlear hair cells are similarly resistant to TEA (Fuchs & Evans, 1990). By contrast, 4-AP eliminated steady voltage oscillations and depolarized the cell by 12 mV, indicating that low frequency oscillations require $I_{K(V)}$ and not $I_{K(Ca)}$. Figure 7*B* shows that resonance in a high frequency cell (206 Hz) is eliminated by TEA and unaffected by 4-AP, indicating that in high frequency cells $I_{K(Ca)}$ and not $I_{K(V)}$ is needed for electrical resonance. In both cells, voltage oscillations were restored following superfusion with normal saline (Fig. 7, bottom traces).

Variations in the relative contribution of $I_{K(V)}$ and $I_{K(Ca)}$ to outward current

The relative contributions of $I_{K(Ca)}$ and $I_{K(V)}$ to the total outward K^+ current in a given hair cell were estimated as follows. Potassium tail currents recorded in response to voltage pulses from ~−50 mV were used to construct steady-state activation curves, which saturate near −30 mV (Art & Fettiplace, 1987). Total K^+ current, I_K, was calculated from the saturating tail current amplitude and assumed to represent current carried by the BK and K_V channels present in each cell:

$$I_K = I_{K(Ca)} + I_{K(V)}. \quad (5)$$

Outward current carried by $I_{K(IR)}$ was not considered, since it carries very little outward current above −30 mV (see Goodman & Art, 1996). The amplitudes of $I_{K(Ca)}$ and $I_{K(V)}$ were derived from experiments such as the one illustrated in Fig. 8, according to:

$$I_K(\alpha,\beta) = \sum_{\alpha}\left(\prod_{\beta}\left(\frac{K_i(\alpha,\beta)}{K_i(\alpha,\beta)+[\beta]}\right)\cdot I_\alpha\right), \quad (6)$$

where the summation is over the set $\alpha = \{BK, K_V\}$, and the product is over the set $\beta = \{4\text{-AP}, TEA\}$. Thus the total current, $I_K(\alpha,\beta)$, is a function of the 4-AP and TEA concentrations, and the apparent affinities, $K_i(\alpha,\beta)$, of each reagent for each channel type. $I_K(\alpha,\beta)$ was measured using test solutions containing 0·035 mM 4-AP, 0·035 mM 4-AP + 0·28 mM TEA, 0·8 mM 4-AP + 0·28 mM TEA, and 0·8 mM 4-AP + 6 mM TEA. Affinity constants were derived from single-cell dose–response curves (Table 2), except for the apparent affinity of K_V channels for 4-AP, which varied according to the time constant of tail current decay (Fig. 4*B*). For each cell, the apparent affinity of K_V for 4-AP was estimated from the time constant of tail current decay according to the empirical relation shown in Fig. 4*B*. The fractional inhibition of $I_{K(Ca)}$ and $I_{K(V)}$ expected for each test solution is given in Table 3. The equations corresponding to eqn (6) for two of the four test solutions were solved simultaneously to determine the unknown quantities $I_{K(Ca)}$ and $I_{K(V)}$.

The size of $I_{K(V)}$, was computed from the amount of tail current suppressed by a low dose of 4-AP (0·035 mM) using eqn (6) (see Fig. 8, column 2). Inhibition by 0·035 mM 4-AP almost certainly reflects blockade of K_V channels since this concentration has no effect on $I_{K(Ca)}$. Equation (6) was used to determine the size of $I_{K(Ca)}$ from the amount of tail current blocked by adding 0·28 mM TEA to a solution containing 0·035 mM 4-AP (Fig. 8, column 3). This

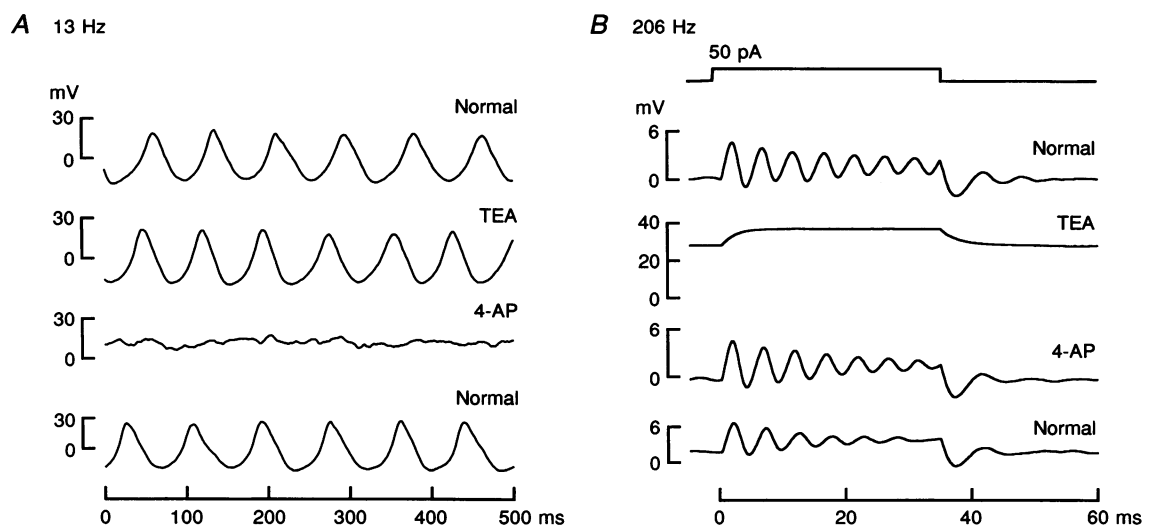

Figure 7. Effect of TEA and 4-AP on resonance in low and high frequency cells

A, steady voltage oscillations in a low frequency cell (13 Hz) in normal saline (Normal), 6 mM TEA (TEA), 0·8 mM 4-AP (4-AP) and returning to normal saline (Normal). Resonant frequency was determined from relative spectral density function, calculated as described in the text. 70 pA injected; ordinate expressed relative to −42 mV. *B*, damped oscillations in response to a 50 pA step in a high frequency cell (206 Hz). Resonance was tested in normal saline (Normal), 6 mM TEA (TEA), 0·8 mM 4-AP (4-AP) and again in normal saline (Normal). Ordinate expressed relative to −47 mV.

Table 3. Fractional inhibition of BK and K_V channels in various solutions

Solution composition		K^+ channel type	
4-AP (mM)	TEA (mM)	BK	K_V 6–60 Hz
0·035	—	—	0·27–0·69
0·035	0·28	0·58	0·27–0·69
0·8	0·28	0·58	0·89–0·98
0·8	6·00	0·95	0·89–0·98

Inhibition of BK and K_V channels by combinations of the K^+ channel blockers, TEA and 4-AP. Fractional inhibition for TEA was calculated from apparent dissociation constants listed in Table 2. Fractional inhibition of K_V channels by 4-AP is given as a range of values calculated from the range of apparent dissociation constants estimated from Fig. 4*B* (legend) for cells tuned between 6 and 60 Hz.

concentration of TEA does not affect $I_{K(V)}$ and so provides a reasonable measure of the amplitude of $I_{K(Ca)}$. Moreover, external TEA and 4-AP are likely to inhibit K^+ channels independently since they are presumed to act at non-overlapping sites. Specifically, external TEA lodges near the external mouth of the ion pore (Heginbotham & MacKinnon, 1992) while 4-AP appears to act by binding to the internal face (Kirsch & Narahashi, 1983).

The sum of $I_{K(V)}$ and $I_{K(Ca)}$ was compared with the total K^+ current measured in normal saline ($n = 30$), the difference being used to calculate percentage error. The general trend was to overestimate the total current, such that the sum of $I_{K(V)}$ and $I_{K(Ca)}$ was between 0·4 and 10% ($n = 25$) greater than the total K^+ current measured initially. Errors of this sort could arise from a gradual decline in current amplitude ('run-down') and cells with errors larger than 10% were omitted from further analysis. Run-down could also lead to the false impression that a particular K^+ channel type was present in a given cell. To test for this possibility, a second estimate of $I_{K(V)}$ and $I_{K(Ca)}$ was obtained, when possible, from the tail current suppressed by 0·8 mM 4-AP and 6 mM TEA (see Fig. 8, columns 4 and 5), respectively. The steady-state K^+ current was used in cells tuned to higher frequencies where the residual tail current was too small to be measured accurately. Thus, two separate measurements of the size of $I_{K(V)}$ and $I_{K(Ca)}$ were obtained in each cell examined, as illustrated in Fig. 8. A given experiment was considered satisfactory if the two estimates of $I_{K(V)}$ and $I_{K(Ca)}$ agreed within 10%. We occasionally observed cells in which the total K^+ current could not be explained by a combination of $I_{K(Ca)}$ and $I_{K(V)}$. The current remaining activated slowly during depolarization and was less steeply voltage dependent than either $I_{K(Ca)}$ or $I_{K(V)}$, increasing e-fold in more than 10 mV. This observation, combined with an apparent sensitivity to TEA that is intermediate between that of $I_{K(Ca)}$ and $I_{K(V)}$, suggests that this residual current was carried by SK channels (Tucker & Fettiplace, 1996).

Figure 8 shows current traces for voltage pulses to −35 mV in three cells exposed to solutions containing 4-AP and TEA, as described above (see Table 3). Test solutions were applied in the order indicated such that the concentration of each antagonist was increased in turn. Results in a cell with a value for f_0 of 223 Hz are shown in Fig. 8*A* and demonstrate resistance to 4-AP (Fig. 8*A*, columns 2 and 4), fractional inhibition of 0·55 by 0·28 mM TEA (Fig. 8*A*, column 3) and nearly complete inhibition by 6 mM TEA (Fig. 8*A*, column 5). The measured suppression by external TEA agrees well with that predicted for $I_{K(Ca)}$, indicating that the majority of K^+ channels in this high frequency cell are BK channels. Figure 8*B* shows a cell with a value for f_0 of 81 Hz in which a slower component of the total outward current was decreased by 0·035 mM 4-AP (Fig. 8*B*, column 2), leaving intact a more rapid portion which could be suppressed by the addition of 0·28 mM TEA (column 3). A combination of 0·8 mM 4-AP and 6 mM TEA was sufficient to inhibit nearly all outward current (Fig. 8*B*, column 5), indicating that outward current is explained by the co-expression of BK and K_V channels. While a total of four cells showed evidence for co-expression of BK and K_V channels, a kinetic difference between the current suppressed by 4-AP and TEA was not always apparent. Results in a lower frequency cell (54 Hz) are shown in Fig. 8*C*; 0·035 mM 4-AP fractionally inhibited 0·76 of the total K^+ current (Fig. 8*C*, column 2) while addition of 0·28 mM TEA had no effect (Fig. 8*C*, column 3). Most outward current was abolished by application of 0·8 mM 4-AP, confirming that this cell contained predominantly K_V channels. We conclude from these results that K_V and BK channels carry outward current in the lowest and highest frequency cells, respectively, and that there exist cells with intermediate resonant frequencies and outward current kinetics that express both K_V and BK channels.

To determine how the conductances $g_{K(V)}$ and $g_{K(Ca)}$ were related to resonant frequency, $I_{K(Ca)}$ and $I_{K(V)}$ were computed from eqn (6) using data from experiments similar to those illustrated in Fig. 8 ($n = 25$), converted to conductance assuming a K^+ equilibrium potential of −86 mV and plotted against f_0 (Fig. 9). Determining this relationship was of interest since it has been shown previously that total K^+ current amplitude increases linearly with resonant frequency (Art & Fettiplace, 1987). Figure 9*A* shows $g_{K(V)}$ amplitude *versus* f_0 in seven cells that contained K_V channels based on the pharmacological separation outlined above and twenty-two cells in which $g_{K(V)}$ was measured in 25 mM TEA, a treatment which blocks all BK channels that might be present and reduces $I_{K(V)}$ by 40%. Measured conductance was corrected for this reduction before plotting the results in Fig. 9*A*. The size of $g_{K(V)}$ increased with f_0 over much of the frequency band in which it was found (~10 and 100 Hz), but declined above 60 Hz. Four cells containing both $g_{K(V)}$ and $g_{K(Ca)}$ are

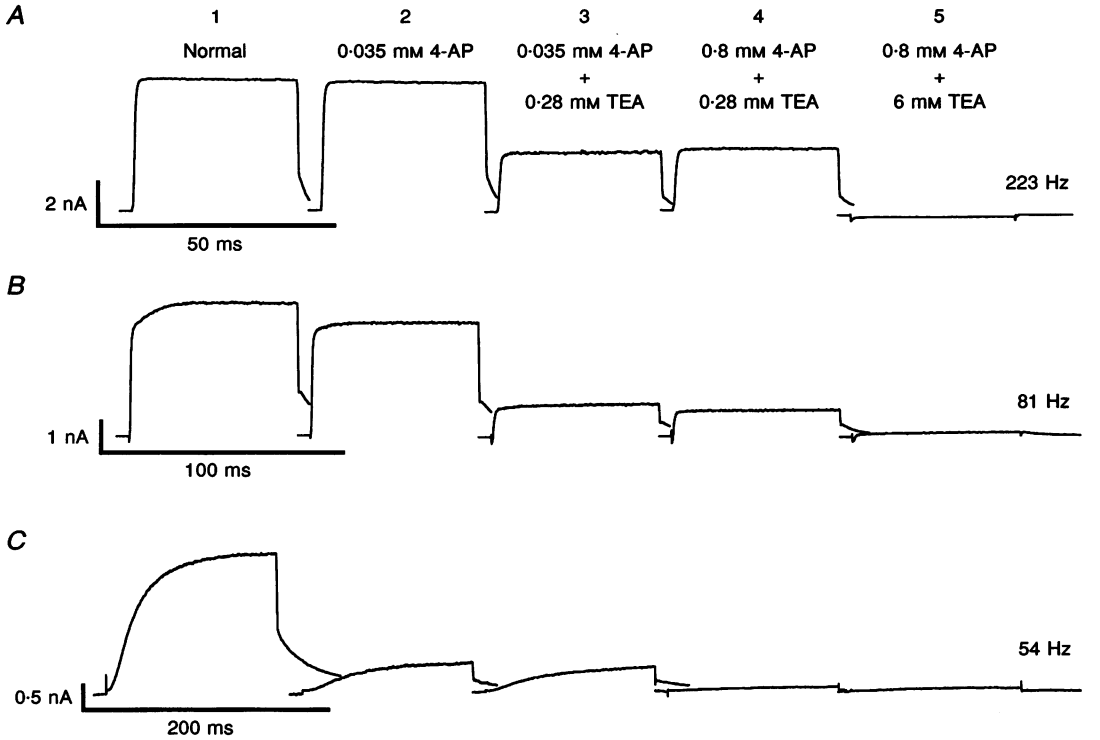

Figure 8. Pharmacological separation of K^+ current in three cells

Each trace shows the current evoked by a pulse to −35 mV. Test solutions were: normal saline (Normal; column 1), 0·035 mM 4-AP; (column 2), 0·035 mM 4-AP + 0·28 mM TEA (column 3), 0·8 mM 4-AP + 0·28 mM TEA (column 4), 0·8 mM 4-AP + 6 mM TEA (column 5). Resonant frequency estimated from the time constant of tail current decay, as described in text. Resonant frequency and holding potentials were 223 Hz and −46 mV in *A*, 81 Hz and −48 mV in *B*, and 54 Hz and −50 mV in *C*. Note that the current and time are scaled differently in each row.

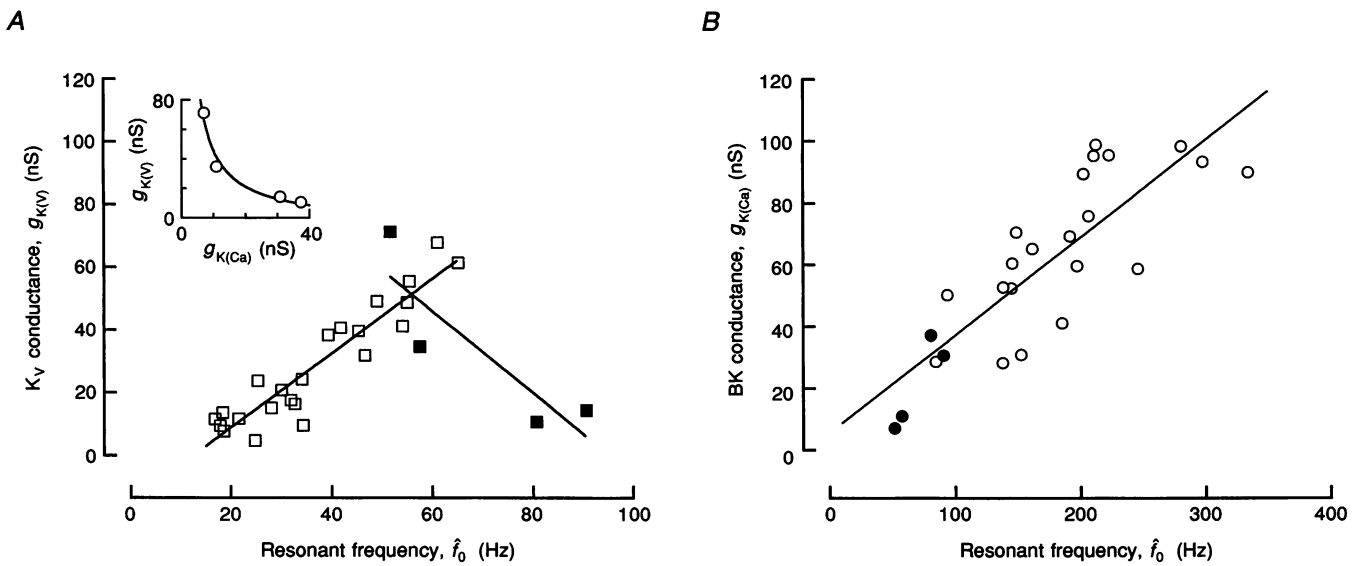

Figure 9. Maximum conductance as a function of resonant frequency, f_0

The sizes of $g_{K(V)}$ and $g_{K(Ca)}$ were determined from the amount of outward current suppressed by 4-AP and TEA, respectively (see text). *A*, the relation between $g_{K(V)}$ and $\hat{f}_0$; ■, the maximum conductance due to K_V channels in 4 cells that contained both K_V and BK channels. Inset shows the relation between $g_{K(V)}$ and $g_{K(Ca)}$ in these cells. *B*, the relation between the $g_{K(Ca)}$ and $\hat{f}_0$; data points (●) indicate the 4 cells that expressed both K_V and BK channels. Straight lines were fitted to the data with correlation coefficients of 0·93 for $g_{K(V)}$ between 10 and 60 Hz and −0·87 between 60 and 100 Hz and 0·83 for $g_{K(Ca)}$.

indicated with filled squares and are distributed near the apparent high frequency limit for $g_{K(V)}$, suggesting an overlap in the expression of K_V and BK channels as a function of resonant frequency. The sizes of $g_{K(V)}$ and $g_{K(Ca)}$ in cells containing both currents are plotted in the inset. The relation between $g_{K(V)}$ and $g_{K(Ca)}$ is hyperbolic, consistent with a fairly smooth transition between cells in which resonant frequency is determined by the kinetics of $I_{K(V)}$ and those employing $I_{K(Ca)}$ for electrical resonance. While it is not possible to exclude expression of K_V channels in hair cells tuned to higher frequencies, if K_V channels are present they carry a current smaller than the 1–2% resolution provided by the pharmacological separations.

As shown in Fig. 9*B*, the size of $g_{K(Ca)}$ determined from pharmacological separation was also correlated to resonant frequency and indicates that $g_{K(Ca)}$ can be detected in cells tuned to more than 50 Hz. Between 50 and 100 Hz, some cells contain a mixture of $g_{K(Ca)}$ and $g_{K(V)}$; the four cells containing both current types are shown as filled circles in Fig. 9*B*. The relation between $g_{K(Ca)}$ and resonant frequency is similar to that determined previously in whole-cell recordings (Art *et al.* 1993) and indicates that $I_{K(Ca)}$ occurs

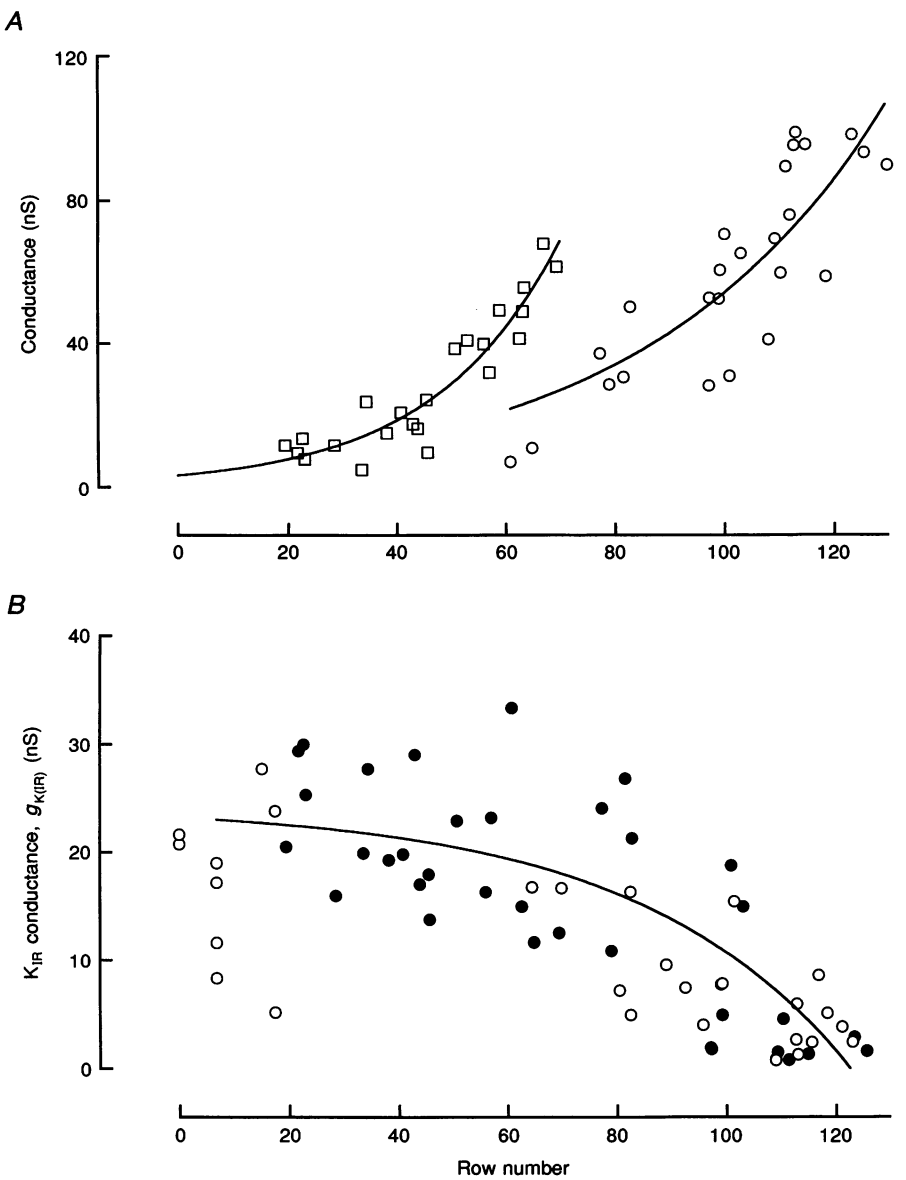

Figure 10. Longitudinal gradients in the number and types of K^+ channels

Resonant frequency was converted to row number, N, using eqn (7), counting from the apex. *A*, the $g_{K(V)}$ (□) and $g_{K(Ca)}$ (○) increase exponentially with N; decline in $g_{K(V)}$ between 60 and 100 Hz omitted for clarity. Smooth curves calculated using $g = g_0 \exp(N/\lambda)$, where g_0 is the conductance at row 0 and λ is a space constant. Coefficients were (g_0, λ): 5·4 nS, 44 rows for $g_{K(Ca)}$; 3·8 nS, 24 rows for $g_{K(V)}$. *B*, the relation between $g_{K(IR)}$ and position was described by $g = g_0(1 - \exp(N/\lambda))$ with $g_0 = 23$ nS and $\lambda = 39$. ●, this study; ○, Goodman & Art (1996).

over the same frequency band as single BK channels (Art *et al.* 1995; Wu *et al.* 1995). The increase in maximum K^+ conductance is likely to be proportional to the number of BK channels and to signal an increase in channel density since single-channel conductance (Art *et al.* 1995; Wu *et al.* 1995) and whole-cell capacitance show little variation as a function of frequency (Art & Fettiplace, 1987).

K^+ channel expression as a function of position

The tonotopic organization of the auditory epithelium results from variations in cellular properties and resonant frequency that are correlated with position along the longitudinal axis. The hair cells in the turtle basilar papilla are arranged in approximately 100 rows. The number of cells per row decreases from a maximum of ~10 at the apex, near the lagena, to a minimum of 2 at the basal end, near the saccule. Frequency is related to position according to:

$$f_0(N) = f_0(0)\exp(N/\lambda), \quad (7)$$

where N is the Nth hair cell row from the apical end, $f_0(0)$ is the resonant frequency at the apex and λ is a space constant having a value of roughly thirty-seven rows. This value of λ corresponds to a distance of approximately 270 μm in adult turtles (Wu *et al.* 1995). A tonotopic map was first drawn by noting the microelectrode position in recordings from higher frequency hair cells in an intact preparation of the turtle cochlea (Crawford & Fettiplace, 1980). Assuming that the mapping described by eqn (7) obtains between 5 and 500 Hz, the data in Fig. 9 were replotted as a function of row number (Fig. 10*A*), assuming a low frequency limit at the apex of 10 Hz. The decline in $g_{K(V)}$ that occurs between 60 and 100 Hz was omitted for clarity.

The smooth curves in Fig. 10*A* describe the exponential relation between row number and K^+ conductance, g, according to

$$g = g_0\exp(N/\lambda). \quad (8)$$

The space constants, λ, derived from this analysis were 43 and 24 rows for $g_{K(Ca)}$ and $g_{K(V)}$, respectively.

In addition to K_V and BK channels, turtle hair cells express K^+-selective inward rectifier, K_{IR}, channels. We have shown previously that $g_{K(IR)}$ is inversely related to resonant frequency (Wu *et al.* 1995; Goodman & Art, 1996). The amplitude of $g_{K(IR)}$ was measured from the chord conductance at −120 mV in the twenty-five cells used in the pharmacological separations, combined with results from a previous study (Goodman & Art, 1996), and plotted against row number in the same manner as for $g_{K(V)}$ and $g_{K(Ca)}$ (Fig. 10*B*). The highest frequency cell in which $I_{K(IR)}$ was detected had a value for f_0 of 290 Hz. The magnitude of $I_{K(IR)}$ was highly variable between experiments; occasionally, $I_{K(IR)}$ could not be detected in any of the cells isolated from a given animal. Thus, the relatively wide variance in $g_{K(IR)}$ apparent in Fig. 10*B* may reflect sensitivity of K_{IR} channels to the cell isolation procedure.

The $g_{K(IR)}$ decreased with row number and the relationship could be described by a function of the form:

$$g = g_0(1 - \exp(N/\lambda)). \quad (9)$$

The space constant for the decrease in $g_{K(IR)}$ amplitude was 39 rows (Fig. 10*B*), comparable to that for the increased expression of BK channels. The variation in conductance for all three channel types reflects differences in the numbers of channels and the exponential relation with distance suggests that a simple mechanism, such as regulation by a diffusible factor (or factors), may orchestrate K^+ channel protein expression in the turtle cochlea.

DISCUSSION

Ensemble of K^+ currents underlying resonance

Different combinations of K^+ currents generate resonance in particular frequency bands. In the lowest decade (6–60 Hz), resonant frequency is determined by the kinetic properties of $I_{K(V)}$, and in the upper decade (60–600 Hz), it is the kinetic properties of $I_{K(Ca)}$ that establish resonant frequency. The expression of BK channels is restricted to this upper decade, in accord with the low frequency limit inferred from modelling single BK channels (Wu *et al.* 1995). In addition, the macroscopic conductance associated with both channel types increases with resonant frequency. This observation is likely to signal an increase in channel number since, at least for BK channels, the single-channel conductance does not vary significantly with resonant frequency (Art *et al.* 1995). While the mechanisms that regulate expression of K^+ channel type and number in the turtle cochlea are unknown, tight control is important for auditory function since both channel number and kinetics contribute to frequency determination (Wu *et al.* 1995).

If BK channel expression were extended to lower frequencies, the relation between maximum conductance and frequency (Fig. 9*B*) predicts that there would be ~100 channels in the lowest frequency cell, assuming a single-channel conductance of 50 pS (Art & Fettiplace, 1987). Since the probability of opening, P_o, is in the order of 0·1 at the resting potential of −50 mV, on average there would be 10 ± 3 channels open with a single-channel current of 1·3 pA. It seems unlikely that a small number of large channels could produce the smooth changes in membrane potential observed in low frequency cells (Figs 1 and 7*A*). Perhaps $I_{K(Ca)}$ is supplanted by $I_{K(V)}$ at low frequencies owing to the smaller single-channel amplitude of the K_V channel (Art *et al.* 1995). The effective single-channel amplitude of K_V channels may be further reduced by a fast, 'flicker' block exhibited by K_V channels in excised membrane patches (J. J. Art & R. Fettiplace, unpublished observations).

A third K^+ channel type, K_{IR}, exists across the entire frequency spectrum and acts in concert with the hair cell Ca^{2+} current to provide positive feedback (Goodman & Art, 1996). $I_{K(IR)}$ is necessary for low frequency resonance (Wu *et*

al. 1995; Goodman & Art, 1996) and its co-expression with K_V channels indicates that the ionic basis of electrical resonance at frequencies less than 50 Hz differs from that previously demonstrated for hair cells employing BK channels (Lewis & Hudspeth, 1983). A similar co-expression has been observed in central regions of the frog posterior canal (Masetto, Russo & Prigioni, 1994), although regenerative behaviour was absent from current clamp recordings. The prevalence of a purely voltage-gated, outwardly rectifying K^+ current is correlated with the generation of spike-like excursions in membrane potential in hair cells of the chick cochlea (Fuchs & Evans, 1990), toadfish saccule (Steinacker & Romero, 1992), and in spiking hair cells identified in the goldfish saccule (Sugihara & Furukawa, 1989). In the chick cochlea, hair cells capable of producing spikes at hyperpolarized potentials generate nearly sinusoidal voltage oscillations when they are maintained at −50 mV (Fig. 1*A*; Fuchs & Evans, 1990). A common mechanism may account for both behaviours, since numerical reconstructions of low frequency resonance in turtle hair cells show that addition of a 1·4 nS transducer conductance is sufficient to depolarize the cell and transform a spiking cell into one that generates sinusoidal oscillations (see Fig. 14 of Wu *et al.* 1995).

Voltage-gated K^+ currents in other hair cell systems

Hair cells in the frog sacculus contain a voltage-gated K^+ current that is completely inactivated by depolarization to −60 mV (Lewis & Hudspeth, 1983; Hudspeth & Lewis, 1988) and was considered an unlikely participant in electrical resonance. However, it is worth noting that the mid-point for inactivation became more negative during the course of their recording (−80 to −93 mV) and is among the most hyperpolarized reported for 4-AP-sensitive currents in hair cells (Hudspeth & Lewis, 1988; Lang & Correia, 1989; Sugihara & Furukawa, 1989; Rennie & Ashmore, 1991; Griguer, Kros, Sans & Lehouelleur, 1993; Murrow, 1994). In contrast, the mid-point for inactivation in turtle hair cells lay between −59 and −45 mV such that a significant fraction of the total K_V channel current is available in the physiological voltage range. Part of the difference might result from alteration of channel properties initiated by F^- in the pipette solutions (Hudspeth & Lewis, 1988). Fluoride ions stimulate G proteins (Sternweis & Gilman, 1982) and could trigger enzymatic cascades that alter the degree of K^+ channel phosphorylation. A role for phosphorylation in the voltage dependence of K^+ channel inactivation is supported by the observation in squid axons that flash photolysis of caged ATP in the presence of protein kinase A shifts inactivation to more depolarized potentials (Perozo, Jong & Bezanilla, 1991).

Voltage-gated K^+ current has been separated into adapting and sustained components in hair cells isolated from the semicircular canals of frog (Housley *et al.* 1989; Masetto *et al.* 1994) and guinea-pig (Rennie & Ashmore, 1991), as well as the chick cochlea (Murrow, 1994), where the adapting component is inhibited by 4-AP with a half-blocking concentration of 0·45 mM (Murrow, 1994). In turtle hair cells, the uniform sensitivity of inactivating and sustained components of the voltage-gated K^+ current to 4-AP argues against the existence of physically distinct ion channels. Interestingly, 5 mM 4-AP was equally effective in reducing both transient and sustained components of outward current in type II vestibular hair cells isolated from the semicircular canals of guinea-pig (Griguer *et al.* 1993).

Inner hair cells of the mammalian cochlea also contain a K^+ current whose resistance to external TEA and sensitivity to 4-AP is reminiscent of $I_{K(V)}$ in turtle hair cells (Kros & Crawford, 1990). Although this pharmacological sketch is consistent with some of the voltage-gated K^+ currents in other hair cells (Lang & Correia, 1989; Steinacker & Perez, 1992; Eatock & Hutzler, 1992; Murrow, 1994; Sugihara & Furukawa, 1995), a thorough comparison based on the pharmacological identity of $I_{K(V)}$ awaits measurement of half-blocking concentrations for TEA and 4-AP in other hair cell systems.

Spatial gradients in K^+ channel expression

The predicted distribution of K^+ channels expressed in cells tuned to low frequency depends on the assumption that a single, monotonic map is sufficient to describe the tonotopic organization of the turtle's cochlea and obscures any variation in K^+ channel expression that might be present across the width of the papilla (see Murrow, 1994). For example, it is possible that K_V expression extends along the longitudinal axis as predicted, but is limited to a relatively narrow strip near one edge of the epithelium. A similar situation obtains in the apical regions of the chick cochlea, where an inactivating, 4-AP-sensitive current is preferentially expressed by the short hair cells located near the abneural edge (Murrow, 1994). Alternatively, K_V channels having different kinetics may be distributed preferentially across the longer hair cell rows located at the apical margin of the basilar papilla. Thus, K_V channels may be expressed in a smaller number of rows than predicted in the present work.

An additional issue concerns the presumptive low frequency limit and the range of resonant frequencies observed in isolated hair cells (10–350 Hz) compared with the intact turtle cochlea (40–600 Hz; Crawford & Fettiplace, 1980). The lack of isolated hair cells tuned to more than 350 Hz is unlikely to result from sampling errors since the range of bundle heights obtained in isolated cells is similar to those found in the intact basilar papilla (Hackney, Fettiplace & Furness, 1993). In addition, the number of hair cell rows predicted from the observed range of resonant frequencies is consistent with the number typically found in the portion of the sensory epithelium overlying the basilar membrane (Sneary, 1988). The agreement in row number is remarkable considering that the number of rows varies between individuals and that the data in Figs 9 and 10 were collected from forty-six different animals. The two maps may be reconciled by assuming that the resonant frequency of

isolated cells is uniformly reduced. In principle, modulation of several cellular properties might underlie a reduction in resonant frequency. These include a slowing of K^+ channel kinetics (Art & Fettiplace, 1987; Hudspeth & Lewis, 1988), modulation of Ca^{2+} diffusion and buffering (Ashmore & Attwell, 1985; Roberts, Jacobs & Hudspeth, 1990) or an increase in cell capacitance. The whole-cell capacitance might increase if either the isolation or recording procedures induce an imbalance in the rates of exocytosis and endocytosis. However, an increase in whole-cell capacitance is unlikely to be the sole explanation, since a 3-fold increase is required to explain a reduction in the maximum resonant frequency from 600 to 350 Hz. Alternatively, a uniform shift towards lower resonant frequencies would result if a constant fraction of the K^+ channels present in each cell are lost during the isolation procedure. This last explanation is attractive in the light of numerical reconstructions of resonance governed by BK channels which indicate that resonant frequency is reduced when fewer channels of identical kinetics are used (Wu *et al.* 1995).

Art, J. J. & Fettiplace, R. (1987). Variation of membrane properties in hair cells isolated from the turtle cochlea. *Journal of Physiology* **385**, 207–242.

Art, J. J., Fettiplace, R. & Wu, Y.-C. (1993). The effects of low calcium on the voltage-dependent conductances involved in tuning of turtle hair cells. *Journal of Physiology* **470**, 109–126.

Art, J. J., Wu, Y.-C. & Fettiplace, R. (1995). The calcium-activated potassium channels of turtle hair cells. *Journal of General Physiology* **105**, 49–72.

Ashmore, J. F. & Attwell, D. (1985). Models for electrical tuning in hair cells. *Proceedings of the Royal Society* B **226**, 325–344.

Crawford, A. C. & Fettiplace, R. (1980). The frequency selectivity of auditory nerve fibres and hair cells in the cochlea of the turtle. *Journal of Physiology* **306**, 377–412.

Eatock, R. A. & Hutzler, M. J. (1992). Ionic currents of mammalian vestibular hair cells. *Annals of the New York Academy of Sciences* **656**, 58–74.

Fuchs, P. A. & Evans, M. G. (1990). Potassium currents in hair cells isolated from the cochlea of the chick. *Journal of Physiology* **429**, 529–551.

Goodman, M. B. (1995). A functional analysis of potassium currents in turtle cochlear hair cells. PhD Dissertation, The University of Chicago, Chicago, IL, USA.

Goodman, M. B. & Art, J. J. (1994). Potassium currents in hair cells isolated from the turtle cochlea. *Society for Neuroscience Abstracts* **20**, 968, 398.4.

Goodman, M. B. & Art, J. J. (1996). Positive feedback by a potassium-selective inward rectifier enhances tuning in vertebrate hair cells. *Biophysical Journal* **71**, 430–442.

Griguer, C., Kros, C. J., Sans, A. & Lehouelleur, J. (1993). Potassium currents in type II vestibular hair cells isolated from the guinea-pig's crista ampullaris *Pflügers Archiv* **425**, 344–352.

Hackney, C. M., Fettiplace, R. & Furness, D. N. (1993). The functional morphology of stereociliary bundles on turtle cochlear hair cells. *Hearing Research* **69**, 163–175.

Heginbotham, L. & MacKinnon, R. (1992). The aromatic binding site for tetraethylammonium ions in potassium channels *Neuron* **8**, 483–491.

Housley, G. D., Norris, C. H. & Guth, P. S. (1989). Electrophysiological properties and morphology of hair cells isolated from the semicircular canal of the frog. *Hearing Research* **38**, 259–276.

Hudspeth, A. J. & Lewis, R. S. (1988). Kinetic analysis of voltage- and ion-dependent conductances in saccular hair cells of the bullfrog, *Rana catesbeiana*. *Journal of Physiology* **400**, 237–274.

Kirsch, G. E. & Drewe, J. A. (1993). Gating-dependent mechanism of 4-aminopyridine block in two related potassium channels. *Journal of General Physiology* **102**, 797–816.

Kirsch, G. E. & Narahashi, T. (1983). Site of action and active form of aminopyridines in squid axon membranes. *Journal of Pharmacology and Experimental Therapeutics* **226**, 174–179.

Kros, C. J. & Crawford, A. C. (1990). Potassium currents in inner hair cells isolated from the guinea-pig cochlea. *Journal of Physiology* **421**, 263–291.

Lang, D. G. & Correia, M. J. (1989). Studies of solitary semicircular canal hair cells in the adult pigeon. II. Voltage-dependent ionic conductances. *Journal of Neurophysiology* **62**, 935–945.

Lewis, R. S. & Hudspeth, A. J. (1983). Voltage and ion-dependent conductances in solitary vertebrate hair cells *Nature* **304**, 538–541.

Masetto, S., Russo, G. & Prigioni, I. (1994). Differential expression of potassium currents by hair cells in thin slices of frog crista ampullaris. *Journal of Neurophysiology* **72**, 443–455.

Murrow, B. W. (1994). Position-dependent expression of potassium currents by chick cochlear hair cells. *Journal of Physiology* **480**, 247–259.

O'Neill, M. P. & Bearden, A. (1995). Laser-feedback measurements of turtle basilar membrane motion using direct reflection. *Hearing Research* **84**, 125–138.

Perozo, E., Jong, D. S. & Bezanilla, F. (1991). Single channel studies of the phosphorylation of K^+ channels in the squid giant axon. II. Nonstationary conditions *Journal of General Physiology* **98**, 19–34.

Press, W. H., Teukolsky, S. A., Vetterline, W. T. & Flannery, B. P. (1994). *Numerical Recipes in C.* Cambridge University Press, Cambridge, UK.

Rabiner, L. R. & Gold, B. (1975). *Theory and Application of Digital Signal Processing.* Prentice-Hall, Englewood Cliffs, NJ, USA.

Rennie, K. J. & Ashmore, J. F. (1991). Ionic currents in isolated vestibular hair cells from the guinea-pig crista ampullaris. *Hearing Research* **51**, 279–292.

Roberts, W. M., Jacobs, R. A. & Hudspeth, A. J. (1990). Colocalization of ion channels involved in frequency selectivity and synaptic transmission at presynaptic active zones of hair cells. *Journal of Neuroscience* **10**, 3664–3684.

Shieh, C.-C. & Kirsch, G. E. (1994). Mutational analysis of ion conduction and drug binding sites in the inner mouth of voltage-gated K^+ channels. *Biophysical Journal* **67**, 2316–2325.

Sneary, M. G. (1988). Auditory receptor of the red-eared turtle: I. General ultrastructure. *Journal of Comparative Neurology* **276**, 573–587.

Snyders, D. J., Tamkun, M. M. & Bennett, P. B. (1993). A rapidly activating and slowly inactivating potassium channel cloned from human heart. *Journal of General Physiology* **101**, 513–543.

Steinacker, A. & Perez, L. (1992). Sensory coding in the saccule: patch clamp study of ionic conductances in isolated cells *Annals of the New York Academy of Sciences* **656**, 27–48.

STEINACKER, A. & ROMERO, A. (1992). Voltage-gated potassium currents and resonance in the toadfish saccular hair cell. *Brain Research* **574**, 229–236.

STERNWEIS, P. C. & GILMAN, A. G. (1982). Aluminum: A requirement for activation of the regulatory component of adenylate cyclase by fluoride. *Proceedings of the National Academy of Sciences of the USA*, **79**, 4888–4891.

SUGIHARA, I. & FURUKAWA, T. (1989). Morphological and functional aspects of two different types of hair cells in the goldfish sacculus. *Journal of Neurophysiology* **62**, 1330–1343.

SUGIHARA, I. & FURUKAWA, T. (1995). Potassium currents underlying the oscillatory response in hair cells of the goldfish sacculus. *Journal of Physiology* **489**, 443–453.

TUCKER, T. R. & FETTIPLACE, R. (1996). Monitoring calcium in turtle hair cells with a calcium-activated potassium channel. *Journal of Physiology* **494**, 613–626.

WU, Y.-C., ART, J. J., GOODMAN, M. B. & FETTIPLACE, R. (1995). A kinetic description of the calcium-activated potassium channel and its application to electrical tuning of hair cells. *Progress in Biophysics and Molecular Biology* **63**, 131–158.

YELLEN, G. (1984). Ionic permeation and blockade in Ca^{2+}-activated K^+ channels of bovine chromaffin cells. *Journal of General Physiology* **84**, 157–186.

Acknowledgements

We thank H. Denison and S. Wen for their technical assistance. This work was supported by National Institutes of Health grant DC00454, an A. P. Sloan Fellowship, and a Brain Research Foundation grant to J. J. A., and a Howard Hughes Predoctoral Fellowship to M. B. G.

Author's present address

M. B. Goodman: Institute of Neuroscience, 1254 University of Oregon, Eugene, OR 97403-1254, USA.

Author's email address

J. J. Art: jart@uic.edu

Received 11 April 1996; accepted 30 August 1996.